Performance evaluation of a parallel-hole collimated detector module for animal SPECT imaging*

HUANG Xian-Chao(黄先超)[1,2,3] ZHANG Zhi-Ming(章志明)[1,2] LI Dao-Wu(李道武)[1,2]
TANG Hao-Hui(唐浩辉)[1,2] LI Ting(李婷)[1,2] LIAO Yan-Fei(廖燕飞)[1,2,3] LIU Jun-Hui(刘军辉)[1,2,3]
WANG Pei-Lin(王培林)[1,2,3] CHEN Yan(陈研)[1,2,3] WANG Ying-Jie(王英杰)[1,2,3]
WEI Long(魏龙)[1,2] SHAN Bao-Ci(单保慈)[1,2] WANG Bao-Yi(王宝义)[1,2;1)]

[1] Key Laboratory of Nuclear Analytical Techniques, Institute of High Energy Physics, Chinese Academy of Sciences, Beijing 100049, China
[2] Beijing Engineering Research Center of Radiographic Techniques and Equipment, Beijing 100049, China
[3] Graduate University of Chinese Academy of Sciences, Beijing 100049, China

Abstract: We have built and investigated a detector module for animal SPECT imaging, especially for use in large field of view (FOV) conditions. The module consists of a PMT-based detector and a parallel-hole collimator with an effective area of 80 mm×80 mm. The detector is composed of a NaI scintillation crystal array coupled to four H8500 position sensitive photomultiplier tubes (PS-PMT). The intrinsic energy resolution of the detector is 11.5% at 140 keV on average. The planar spatial resolution of the module changes from 2.2 mm to 5.1 mm at different source-to-collimator distances with an unchanged sensitivity of about 34cps/MBq. Additionally, the SPECT Micro Deluxe Phantom imaging was performed with a radius of rotation (ROR) of 40 mm. Using the FBP reconstruction algorithm, a high performance image was obtained, indicating the feasibility of this detector module.

Key words: animal imaging, SPECT parallel-hole collimator

PACS: 87.57.uh, 87.57.cf **DOI:** 10.1088/1674-1137/35/12/016

1 Introduction

With advances in cell biology and transgenic technology, the in vivo molecular imaging of small animals has become a focus of current scientific research [1, 2]. Some dedicated small animal single photon emission computed tomography (SPECT) systems have been developed [3–6].

Sub-millimeter spatial resolution can be obtained by using a pinhole collimator when the object is placed close to the pinhole [3, 4]. Due to the magnification effect, the FOV is usually small considering the restrictions of detector size and acceptance angle [7]. When a large FOV is needed, the object must be placed away from the pinhole, which leads to a low spatial resolution and sensitivity. So when the resolution requirements are not stringent and a large FOV is needed, a high resolution parallel-hole collimator is available. Others have investigated the application of compact detectors with a parallel-hole collimator for SPECT [8, 9].

We have built a detector module for animal SPECT imaging using a PMT-based detector and a parallel-hole collimator. The performances of intrinsic energy resolution, planar spatial resolution and sensitivity are tested in this paper.

2 System description

The collimator is composed of a closely packed array of hexagonally shaped holes. The diameter (for hexagonal holes, the perpendicular "face-to-face" distance) and the length of the holes are 1.2 mm and 27 mm separately, and the thickness of the septa is 0.16 mm with lead material.

The detector consists of a NaI crystal array

Received 24 January 2011, Revised 9 March 2011
* Supported by Natural Science Foundation of China (10805049, 10775149)
1) E-mail: wangboy@mail.ihep.ac.cn

and four H8500 PMTs coupled together with silicon grease. The crystal array is of a 62×62 matrix with the pixel size 1.4 mm×1.4 mm×6 mm. The gap width is 0.2 mm filled with a reflector material. The H8500 PMT has an 8×8 array of anodes with an external size of 52 mm×52 mm. The active area is 49 mm×49 mm, which means that the effective area is 89%. When four H8500s join together, the dead gap between two tubes is about 6 mm.

The sketch map of the readout electronics is shown in Fig. 1. The 256 anode outputs of the PMTs are read out into four signals ($X-$, $X+$, $Y-$, $Y+$) using a symmetric charge division (SCD) method combined with the charge division circuit developed by Popov [10, 11]. After amplification and shaping, the four signals are fed into the DAQ board, where continuous sampling and digitization are performed. These digital values are used to calculate the position using the centroid method. The raw image of the Tc-99 m flood source is shown in Fig. 2(a). The result indicates that the scintillation crystal array has an effective area of more than 50×50 pixels and that the dead gaps of the joint parts of PS-PMTs are still available for detection.

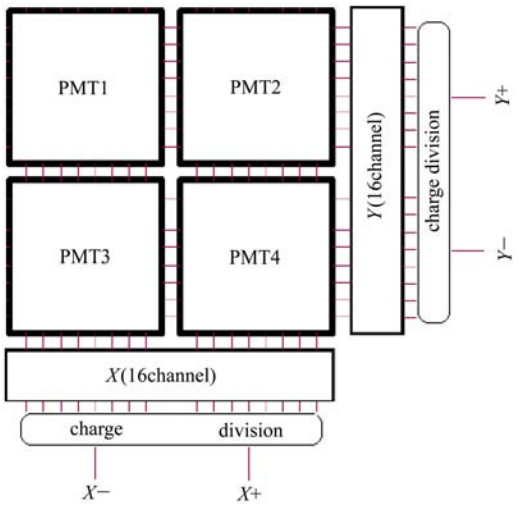

Fig. 1. The sketch map of readout electronics.

Because of the spatially non-uniform response of the PSPMT, the crystal positions are distorted in the raw image. However, the relative position of individual crystals in the matrix is known and the clusters of events corresponding to individual crystals can be resolved in the raw image. A crystal position look-up table can be constructed in Fig. 2(b). Corrections to the raw image are then performed by mapping the data identified to belong to a particular crystal. Finally the energy of the events can be calculated by summing the four output signals and the energy spectrum can be counted for individual crystals.

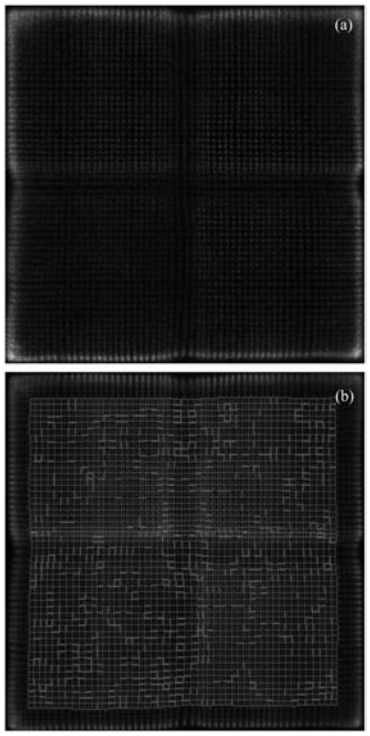

Fig. 2. The detector image. (a) The raw image of Tc-99m flood source; (b) the mapped region of the crystals.

3 Performance characteristics

3.1 Intrinsic energy resolution

When the crystal position look-up table is constructed, the energy spectrum of individual crystals is acquired by using a Tc-99 m flood source with the collimator demounted. The energy resolution is defined as the ratio of the FWHM of the energy spectrum to the energy of peak according to the NEMA standards. By fitting a Gaussian function to the profile of the energy spectrum, the FWHM can be obtained. The energy spectrum and the Gaussian fitting curve of a single crystal is shown in Fig. 3. The average energy resolution of our detector is 11.5%.

3.2 Planar spatial resolution

As currently there are no test standards for animal SPECT, we adopted the NEMA standard for clinical SPECT to perform the test. The planar spatial resolution is measured with a line source made from a glass capillary tube filled with Tc-99 m. The inner diameter of the tube is 0.5 mm. The line source is imaged at various source-collimator distances from 10 mm to 60 mm for 80 seconds separately. A ±10% energy window is used.

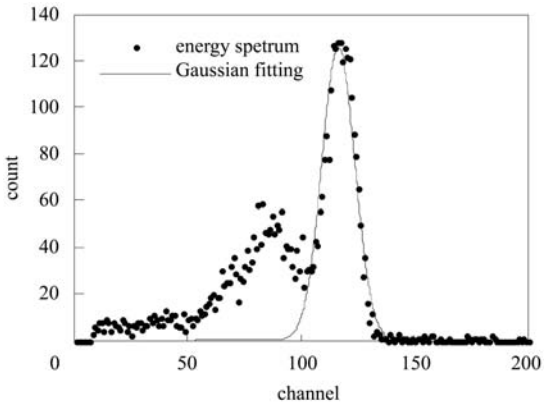

Fig. 3. The energy spectrum of one crystal.

Projection images at various distances are shown in Fig. 4. As the distance increases, the profile of the images broadens, representing the degradation of spatial resolution. We defined the planar spatial resolution as the FWHM of the line spread functions fitted by a Gaussian function. The values are calculated in Table 1.

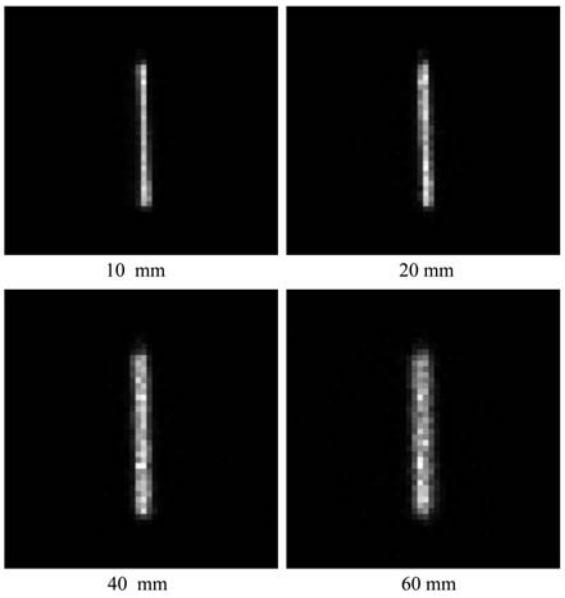

Fig. 4. Projections of the line source.

Table 1. Planar spatial resolution.

distances/mm	resolution/mm
10	2.2
20	3.3
40	3.8
60	5.1

3.3 Sensitivity

The sensitivity is defined as the ratio of the counts detected in one acquisition plane to the activity of the source. A Tc-99 m cylindrical source is placed above the center of the module with an activity of 6MBq. The cylindrical source is 4 mm in diameter and 3 mm in length. The values in different source-collimator distances are calculated in Table 2, where a ±10% energy window is also used.

Table 2. Sensitivity.

distances/mm	sensitivity(cps/MBq)
10	38
20	34
40	34
60	34

3.4 Phantom reconstruction

The Micro Deluxe Phantom shown in Fig. 5 is imaged using this module. The phantom has an outer diameter of 5 cm, the diameters of the rods in the six sectors are 4.8, 4.0, 3.2, 2.4, 1.6 and 1.2 mm, and the center-to-center spacing is two times the rod diameter. The phantom is filled with a Tc-99 m solution of 4mCi. 120 projection views are acquired at 80s/view with the ROR of 40 mm. The images are reconstructed using the filtered back-projection reconstruction algorithm [12].

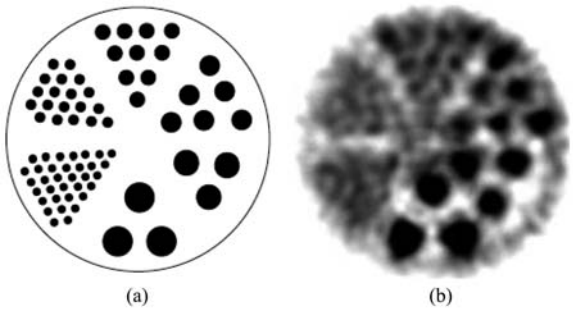

Fig. 5. The reconstruction of the phantom. (a) The sketch map of the phantom; (b) the tomographic image of the phantom.

The tomographic image of the axial section of the phantom is shown in Fig. 5(b) where the largest 3 sectors are easily discriminated. The normalized calibration and center of rotation correction are taken into consideration. The geometrical offset exists due to the effect of scattering and attenuation, the geometrical error of the gantry, the precision of the reconstruction algorithm and so on.

4 Discussion

The experimental result of the planar spatial resolution is drawn in Fig. 6. The data is fitted linearly with a coefficient of determination of 0.9256,

indicating that the spatial resolution decreases in linearity approximately with the increase of the source-collimator distance. On the other hand, as the source-collimator distance increases, the sensitivity is almost unchanged, varying from 34 to 38cps/MBq. Both results are consistent with the analytic formulas [13].

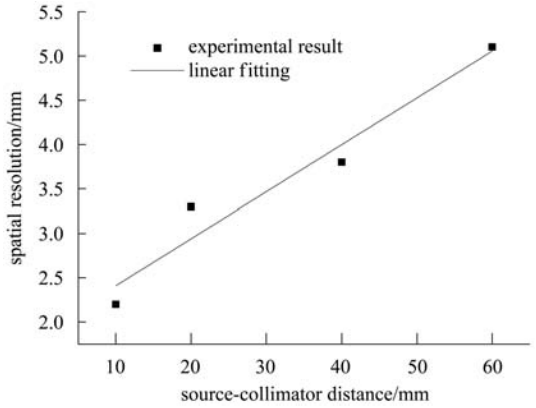

Fig. 6. The curve of resolution.

Although imaging with a pinhole collimator can achieve a spatial resolution of sub-millimeters, there are many restrictions. For high resolution, the object must be placed close to the pinhole, leading to a restriction of the object dimensions. When the resolution requirements are not stringent, the object can be placed away from the pinhole to obtain enough FOV, but the sensitivity drops rapidly.

The effective detector area of more than 50×50 pixels makes sure that our detector module can image an object with a FOV of 80 mm×80 mm which is several times larger than using pinhole collimator. Although the spatial resolution decreases as the source-collimator distance increases, a resolution of 5.1 mm can still be achieved at a 60 mm source-to-collimator distance and the sensitivity is almost unchanged.

The Micro Deluxe Phantom is also reconstructed with the radius of rotation of 40 mm shown in Fig. 5(b). The sector of 3.2 mm is easily discriminated, indicating the feasibility of this detector module in large FOV imaging.

By preliminary evaluation, our detector module can achieve a high resolution from 2.2 mm to 5.1 mm, which is adaptable for both near and far imaging distances with a proper sensitivity. In vivo imaging of animals will be performed in the next step.

References

1 King M A et al. Journal of Cellular Biochemistry Supplement, 2002, **39**: 221
2 Alberto Del Guerra et al. Nuclear Instruments and Methods in Physics Research A, 2007, **583**: 119
3 Beekman F J et al. Journal of Nuclear Medicine, 2005, **46**: 1194
4 Kubo N et al. Annals of Nuclear Medicine, 2005, **19**: 633
5 Bradley E L et al. IEEE Transactions on Nuclear Science, 2006, **53**: 59
6 Choong W S et al. IEEE Transactions on Nuclear Science, 2005, **52**: 174
7 SONG T Y et al. IEEE Transactions on Nuclear Science, 2003, **50**: 327
8 Choong W S et al. IEEE Transactions on Nuclear Science, 2002, **49**: 2228
9 Schramm N et al. IEEE Transactions on Nuclear Science, 2002, **47**: 1263
10 Popov V et al. IEEE Nuclear Science Symposium Conference Record, 2003, **3**: 2156
11 Popov V et al. IEEE Nuclear Science Symposium Conference Record, 2001, **4**: 1937
12 Lauritsch G et al. Proc. SPIE, 1998, **3338**: 1127
13 Anger H. Journal of Nuclear Medicine, 1964, **5**: 51